

1 **Multi-objective optimisation of material properties and strut geometry for** 2 **poly(L-lactic acid) coronary stents using response surface methodology**

3 R.W. Blair^{a,*}, N.J. Dunne^{b-f}, A.B. Lennon^a, G.H. Menary^a

4 ^a *School of Mechanical and Aerospace Engineering, Queen's University, BT9 5AH, Belfast, UK*

5 ^b *School of Mechanical and Manufacturing Engineering, Dublin City University, Dublin 9, Ireland*

6 ^c *Centre for Medical Engineering Research, School of Mechanical and Manufacturing Engineering,*
7 *Dublin City University, Dublin 9, Ireland*

8 ^d *School of Pharmacy, Queen's University, Belfast, BT9 7BL, UK*

9 ^e *Trinity Centre for Bioengineering, Trinity College Dublin, Dublin 2, Ireland*

10 ^f *Advanced Materials and Bioengineering Research Centre (AMBER), Royal College of Surgeons in*
11 *Ireland and Trinity College Dublin, Dublin, Ireland.*

12 **Abstract**

13 Coronary stents for treating atherosclerosis are traditionally manufactured from metallic alloys.
14 However, metal stents permanently reside in the body and may trigger undesirable immunological
15 responses. Bioresorbable polymer stents can provide a temporary scaffold that resorbs once the
16 artery heals but are mechanically inferior, requiring thicker struts for equivalent radial support,
17 which may increase thrombosis risk. This study addresses the challenge of designing mechanically
18 effective but sufficiently thin poly(L-lactic acid) stents through a computational approach that
19 optimises material properties and stent geometry. Forty parametric stent designs were generated:
20 cross-sectional area (post-dilation), foreshortening, stent-to-artery ratio and radial collapse pressure
21 were evaluated computationally using finite element analysis. Response surface methodology was
22 used to identify performance trade-offs by formulating relationships between design parameters
23 and response variables. Multi-objective optimisation was used to identify suitable stent designs from
24 approximated Pareto fronts and an optimal design is proposed that offers comparable performance
25 to designs in clinical practice. In summary, a computational framework has been developed that has
26 potential application in the design of high stiffness, thin strut polymeric stents that contend with the
27 performance of their metallic counterparts.

28 **Corresponding address: School of Mechanical and Aerospace Engineering, Queen's University, Ashby Building, Stramillis Rd, Belfast BT9*
29 *5AG, UK. Tel.: +44 (0)28 9097 5523. E-mail address: rblair522@qub.ac.uk (R. Blair)*

30 1. Introduction

31 Balloon angioplasty, performed by Andreas Grüntzig in 1977, is recorded as the first successful effort
32 to treat an occluded coronary artery and subsequently revolutionised the treatment of coronary
33 artery disease.^[1] However, the surgical procedure suffers from significant limitations, namely vessel
34 occlusion and restenosis, which prompted the development of the first bare metal stent (*BMS*)
35 nearly a decade later.^[2] Whilst *BMSs* reduced the incidence rate of restenosis when compared to
36 balloon angioplasty, the introduction of a permanent metallic cage provoked neointimal hyperplasia,
37 an inflammatory response of the vessel walls^[3], and as a result drug-eluting stents (*DESs*) succeeded
38 *BMSs*, containing a durable polymer coating which releases an antiproliferative drug (e.g. sirolimus
39 or paclitaxel) that attenuates intra-stent neointimal proliferation^[4]. Drug-eluting stents have shown
40 reduced restenosis rates when compared to *BMSs*.^[5,6] However, they suffer from inherent flaws
41 based on the permanent nature of their design and issues have been reported regarding the long-
42 term (> 1 year) safety of these devices including delayed healing and late stent thrombosis (*LST*)^[7,8,9],
43 which has prompted the development of bioresorbable stents (*BRSs*). Bioresorbable stents provide
44 short-term scaffolding to the arterial wall until it has healed and are subsequently resorbed, offering
45 superior conformability and flexibility to their permanent metallic counterparts, whilst enabling late
46 luminal gain, late expansive remodelling and potentially reducing the risk of *LST* associated with
47 *DESs* following resorption.^[10,11]

48 Whilst polymeric *BRSs* present a clinically attractive option, they require wider and thicker struts to
49 provide an equivalent level of arterial support (Table 1) when compared to their metallic
50 counterparts. As a result, polymeric *BRSs* have higher stent-to-artery ratios,^[12,13] which have been
51 shown to increase the risk of myocardial infarction, thrombosis and restenosis.^[14,15] A thick-strut
52 design also limits the diameter a stent can be crimped to, resulting in an increased crossing-profile
53 that hinders the deliverability of the device^[16] and restrict normal vasomotion.^[4] Additionally,
54 polymeric *BRSs* demonstrate higher degrees of foreshortening (due to an increased strut length)

55 during deployment, which can initiate vascular restenosis injuries.^[17] Improvements in material
56 processing, coupled with the correct matching of the stent geometry to the material may produce
57 polymeric *BRSs* with reduced strut thickness and comparable performance to current generation
58 metallic *DESs*.^[18–20]

59 **Table 1.** Comparison of strut geometry and performance metrics of clinically tested bioresorbable
60 stents (*BRSs*) and modern metallic drug-eluting stents (*DESs*) for coronary application.^[4,12,20–25]

	<i>Polymeric BRSs</i>	<i>Metallic DESs</i>
Strut thickness (μm)	125–156	80–140
Strut width (μm)	140–216	80–132
Stent-to-artery ratio (%)	26.0–32.0	15.5–21.4
Crossing profile (mm)	1.2–1.7	1.0–1.2

61
62 The elastic modulus of the polymer, which affects the radial collapse pressure of the stent, may
63 potentially be the most important parameter in polymeric *BRS* design.^[20,26] Pauck and Reddy^[20]
64 performed computational bench testing on three commercially available stent geometries, whilst
65 varying the elastic modulus of the platform material, poly(L-lactic acid) (*PLLA*). The authors
66 concluded that using a geometry similar to that of the Absorb *BVS* (Abbott Vascular, USA), with a
67 strut thickness and a strut width of 100 μm , coupled with an elastic modulus of 9 GPa, allows the
68 desired collapse pressure of at least 40 kPa to be met.^[18] The elastic modulus of extruded *PLLA* is
69 approximately 3 GPa,^[27] which is significantly lower than the required value of 9 GPa, and hence
70 additional processing steps must be taken to improve upon this.

71 Stretch blow moulding (*SBM*) is a processing technique used in the production of *BRS* to improve the
72 elastic modulus of the polymer.^[27,28] In the *SBM* process, the polymer is initially extruded into a
73 thick-walled tube (parison) and heated above its glass transition temperature during which it is
74 biaxially stretched to create a thin-walled tube with improved mechanical properties.^[29] Whilst a

75 three-fold increase in the elastic modulus is difficult to physically attain, Blair et al.^[30] showed that by
76 tailoring processing parameters, biaxial stretching can improve the elastic modulus and yield
77 strength of extruded *PLLA* sheet by approximately 80% and 70%, respectively. Given that the
78 relationship between elastic modulus and strut thickness has been shown to be nonlinear,^[26]
79 through careful matching of material properties to stent geometry, a physically attainable elastic
80 modulus may be used to meet the radial stiffness threshold with a minimal increase in strut
81 thickness.

82 The mechanical performance and efficacy of a stent design is strongly dependent on the
83 configuration of strut geometry.^[31–33] Finite element analysis is an especially prevalent technique
84 within the discipline of computational biomechanics, where *in vivo* testing is exceptionally
85 challenging, and may be used as preclinical testing tool to optimise stent geometry prior to any form
86 of physical testing.^[31,34] To evaluate the performance and efficacy of a given stent design, simulated
87 tests are typically conducted in which one (or more) metrics are assessed across a range of
88 potentially viable stent geometries. Stent geometries may be parameterised in terms of strut width,
89 strut thickness, strut length and connector shape^[35] whilst performance metrics fall under two main
90 headings: (i) dilation metrics and (ii) mechanical metrics. Dilation metrics are concerned with the
91 behaviour of the stent during (and immediately following) inflation, with radial recoil, foreshortening
92 and stent-to-artery ratio amongst the most commonly evaluated metrics.^[32,36] Mechanical metrics
93 are concerned with the performance of the expanded stent, with radial stiffness considered as the
94 most important mechanical metric for polymeric stents.^[20]

95 It is difficult to define what constitutes an optimal stent design, given that the definition of ‘optimal’
96 depends on the parameters investigated and the performance metrics assessed. The ideal stent is
97 typically considered as one that is highly deliverable with thin-struts (to improve delivery through
98 tortuous vascular paths) but with high radial stiffness and minimal elastic recoil, to resist
99 restenosis.^[37] However, this statement in itself presents a number of conflicting requirements and as

100 a result, an optimised design will always be a trade-off. This is evident from a cross-comparison of
101 the parametric studies conducted by García et al.,^[38] Li et al.,^[39] Migliavacca et al.,^[32] Pant et al.^[40]
102 and Timmins et al.^[41] Radial stiffness and radial recoil were improved by increasing strut width and
103 strut thickness whilst decreasing strut length, however this often came at the expense of the stent-
104 to-artery ratio and foreshortening.

105 In summary, improvements in *PLLA* stent design may be attained using a combination of two factors:
106 (i) enhancing mechanical properties of the platform polymer by tailoring its processing history and
107 (ii) iteratively refining the stent's shape by modifying key geometric features. Few studies have
108 considered the combined effect of the processing history and stent geometry in order to optimise
109 stent performance.^[39,42] Furthermore, to the best of the authors' knowledge, no study has
110 considered the combined effect of the biaxial stretching processing history and the geometric
111 configuration when optimising the mechanical performance of a coronary stent. This study aims to
112 address this challenge of designing mechanically effective but sufficiently thin bioresorbable *PLLA*
113 stents through multi-objective optimisation of material parameters and stent geometry.

114 **2. Material and methods**

115 The design of *PLLA* stents may be improved by enhancing the material properties of the platform
116 polymer through biaxial stretching and iteratively refining the stent geometry. By parameterising
117 these design inputs and computationally evaluating the performance of a given stent design across a
118 series of metrics (that capture the conflicting requirements for a stent), empirical relations were
119 established that relate both the stent processing history and geometry to its performance. Using
120 these empirical relations, performance trade-offs were identified and an optimal design may be
121 identified through multi-objective optimisation.

122 2.1 Process parametrisation

123 In a previous study by Blair et al.^[30], the *SBM* process was idealised and replicated using a custom-
124 built biaxial tensile tester, to evaluate the mechanical properties of *PLLA* pre- and post-biaxial
125 stretching. The elastic modulus (E) and yield strength (σ_Y) of extruded *PLLA* sheet increased by
126 approximately 80% and 70% following biaxial stretching. These mechanical properties were
127 observed to be highly dependent on the stretch ratio in the machine direction (*MD*), λ_{MD} , and the
128 stretch ratio in the transverse direction (*TD*), λ_{TD} , in addition to the aspect ratio (A_r) between the
129 pair, defined as the quotient of λ_{TD} and λ_{MD} (Fig. 1).

130 In a follow-on study, Blair et al.^[43] varied A_r and performed uniaxial tensile testing at various
131 temperatures (20, 37 and 55 °C) and extension rates (1, 5 and 10 mm/min) — comparable conditions
132 to those experienced by a stent.^[44] By tailoring A_r , biaxially stretched sheets were processed with
133 direction dependent (anisotropic) mechanical properties (Fig. 1). Results also showed that these
134 mechanical properties were strongly dependent on temperature during uniaxial deformation, and
135 not heavily dependent on extension rate. Empirical relations were developed that related E and σ_Y to
136 A_r (Eq. 1–4) for $0.4 \leq A_r \leq 2.3$ and for a temperature of 37 °C (Fig. 2), and a transversely isotropic,
137 rate-independent, elastic-plastic constitutive model was calibrated against uniaxial tensile test data.
138 A simplified version of this model is proposed in the present study (Fig. 3) which neglects the
139 softening following yield and assumes *PLLA* exhibits perfectly plastic behaviour, i.e. a change in
140 strain causes no observable change in stress.

141

142 **Fig. 1.** Schematic diagram showing experimental characterisation (from uniaxial tensile testing at
143 37 °C and 5 mm/min) for various aspect ratios (A_r) of biaxially stretched *PLLA*.

$$E_{MD} = 3750 - 927A_r \quad (1) \quad \sigma_{Y,MD} = 71 - 14A_r \quad (2)$$

$$E_{TD} = 1584 + 944A_r \quad (3) \quad \sigma_{Y,TD} = 37 + 14A_r \quad (4)$$

144

145 **Fig. 2.** Graphical representation of constitutive equations showing (a) elastic modulus (E) and (b)
146 yield strength (σ_y) in both the machine direction (MD) and transverse direction (TD) as a function of
147 aspect ratio (A_r).

148 Given that one of the most challenging aspects to overcome when designing polymer-based stents
149 lies in the significantly lower radial stiffness compared to their metallic counterparts, it may be
150 beneficial to process the stent such that it has a preferential circumferential orientation. An $A_r > 1$
151 generated stent designs that are stiffer in the circumferential direction, whilst an $A_r < 1$ generated
152 stent designs that are stiffer in the longitudinal direction (Fig. 3).

153

154 **Fig. 3.** Schematic diagram showing the constitutive model stress-strain (σ - ϵ) curves for an $A_r > 1$,
155 which generates stents that are stiffer in the circumferential direction, and an $A_r < 1$, which
156 generates stents that are stiffer in the longitudinal direction.

157 **2.2 Geometry parametrisation**

158 The stent geometry used in the present study was based on a conventional open-cell stent design
159 with straight bridges, using SolidWorks 2016 (Dassault Systèmes, France) to generate the three-
160 dimensional model (Fig. 4). The stent was designed in the crimped state with two repeating unit cells
161 used to represent the full-length stent geometry, thereby reducing computational cost. Parametric
162 stent geometries were generated by varying the strut width (w), the strut thickness (t) and the strut
163 length (l).

164

165 **Fig. 4.** Geometry parameterisation in terms of strut width (w), strut thickness (t) and strut length (l).

166 2.3 Performance metrics

167 Four performance metrics were extracted for each stent design, based on the results of deployment
168 and bench test simulations: (i) the cross-sectional area post-dilation (*CSA*), (ii) foreshortening (*FS*),
169 (iii) stent-to-artery ratio (*SAR*) and (iv) radial collapse pressure (*RCP*). Initially, an idealised quasi-
170 static expansion procedure was simulated in Abaqus/Standard 2016 (Dassault Systèmes, USA) using
171 a displacement driven cylinder (meshed with S4R shell elements) and a deformable solid stent
172 (meshed with C3D8R brick elements). The stent was designed in a pre-crimped state (Fig. 5a) and
173 constrained in both the axial and tangential directions (with respect to a user-defined cylindrical
174 coordinate system) via three nodes forming an equilateral triangle in the central section. A radial
175 displacement was prescribed to all nodes on the cylinder increasing the stent diameter from 1.8 mm
176 to 3.5 mm using the smooth-step amplitude definition within Abaqus, with tangential and axial
177 displacement prohibited (Fig. 5b). Frictionless surface-to-surface contact was assumed, and self-
178 contact was enabled for the stent. Following expansion, the cylinder was contracted during which
179 the stent recoiled (Fig. 5c). The time-frame typically required for polymeric stent expansion
180 approaches 1 min according to published guidelines from Abbott.^[45] However, given that a rate-
181 independent material model is used, the time frame for expansion was reduced to 1 s.

182

183 **Fig. 5.** Finite element deployment simulation showing the stent in its (a) initial crimped state;
184 (b) deployed (expanded) state and (c) final (recoiled) state.

185 The *CSA* following unloading was calculated based on the internal diameter of the stent (D_{unload})
186 (Eq. 5) (Fig. 6a). During expansion, the opening of the strut hoops naturally cause the stent to
187 contract in the axial direction (Fig. 6b). The *FS* of a stent was defined as the percentage reduction
188 between the stent length in its crimped state ($L_{initial}$) and the stent length following unloading (L_{unload})
189 (Eq. 6). The *SAR* of the stent (Fig. 6c) was calculated as the ratio between the external surface area of
190 the stent in its crimped state ($SA_{initial}^{stent}$) and the internal surface area of a compatible cylindrical artery

191 (SA^{artery}) (Eq. 7). The RCP of an expanded stent was evaluated through an additional virtual bench
 192 test in which eight rigid plates (meshed with R3D4 elements) (Fig. 6d) were radially contracted using
 193 a displacement driven process to produce 10% diameter loss. The RCP was calculated as the
 194 quotient of the average reaction force acting on the plates (RF_{ave}) and the surface area of the stent
 195 post-recoil (SA_{unload}^{stent}) (Eq. 8). The smooth-step amplitude definition was used with frictionless surface-
 196 to-surface contact between the plates and the stent, and self-contact was enabled for the stent.

197

198 **Fig. 6.** Schematic representations of tests for: (a) cross-sectional area (post-dilation), CSA ;
 199 (b) foreshortening, FS ; (c) stent-to-artery ratio, SAR and (d) radial collapse pressure, RCP .

$$CSA = \pi \left(\frac{D_{unload}}{2} \right)^2 \quad (5)$$

$$FS = \frac{L_{initial} - L_{unload}}{L_{initial}} \times 100\% \quad (6)$$

$$SAR = \frac{SA_{initial}^{stent}}{SA^{artery}} \times 100\% \quad (7)$$

$$RCP = \frac{RF_{ave}}{SA_{unload}^{stent}} \quad (8)$$

200

201 2.4 Optimisation

202 The time required to perform the finite element simulations and calculate the performance metrics
 203 for a given parametric stent design exceeded 1 h using five parallel processors. At these time scales,
 204 global optimisation processes become computationally inefficient and the majority of optimisation
 205 studies tend to adopt surrogate modelling approaches.^[35] Hence, response surface methodology
 206 (RSM) was employed to provide an empirical correlation between processing and geometry
 207 parameters and the mechanical performance of the stent.

208 A design space was established using the limits for each of the design parameters (Table 2). The
 209 lower limit of A_r generates stents that are stiffer in the axial direction whilst the upper limit
 210 generates stents that are stiffer in the circumferential direction. A lower limit of 100 μm was set for
 211 w and t to generate geometries that resembled a metallic stent, whilst an upper limit of 200 μm was
 212 set to generate geometries that resembled a polymeric stent. An upper limit of 1200 μm was set for l

213 to avoid self-contact between neighbouring circumferential rings, whilst a lower limit of 900 μm was
214 set to prevent excessive plastic deformation. A baseline design was generated by setting A_r , w , t and
215 l at the midpoint of their range.

216 **Table 2.** High and low levels for design parameters (A_r , w , t and l).

A_r (-)	w (μm)	t (μm)	l (μm)
0.4	100	100	900
2.3	200	200	1,200

217

218 Initially, 40 design points that uniformly filled the design space were selected using an optimised
219 Latin hypercube (LHC) sampling technique.^[46] Parametric stent designs and finite element models
220 were automatically generated using a combination of Python (version 2.7.13; Python Software
221 Foundation) scripting, SolidWorks 2016 (SolidWorks Corporation, USA) and the Abaqus CAE pre-
222 processor. Deployment and bench testing simulations were performed in order to compute discrete
223 values for each performance metric (CSA , FS , SAR and RCP). Multiple linear regression analysis was
224 performed on the results using R (version 3.4.0)^[47] to provide an empirical correlation between each
225 performance metric and design parameters. The Matplotlib (version 2.2.2) package^[48] was used to
226 generate three-dimensional response surface plots to provide a qualitative, visual assessment of the
227 results.

228 Following the RSM, multi-objective sequential least squares optimisation was performed in Python
229 using the NumPy (version 1.14.2)^[49] and SciPy packages (version 1.2.0)^[50] to identify suitable options
230 from non-dominated Pareto designs, i.e. a design that cannot be improved without degrading at
231 least one of the other performance metrics. Each performance metric was normalised (scaled) to the
232 same range [0,1], based on its minimum and maximum attainable values, attained through single
233 objective sequential least squares minimisation. A single objective function (OF) was constructed
234 (Eq. 9) that combines these normalised CSA , FS , SAR and RCP terms, with each parameter assigned
235 an equal weighting. The intention of this optimisation was to minimise FS and SAR whilst maximising

236 CSA and RCP. Hence, negative sign convention was adopted for CSA and RCP so that lower values for
237 absolute and normalised performance metrics indicate better designs. An inequality constraint was
238 imposed that prevented RCP dropping below 40 kPa (Eq. 10), which is commonly considered the
239 minimum allowable collapse pressure for coronary stents.^[18] An additional inequality constraint was
240 imposed that prevented t from exceeding the baseline value of 150 μm (Eq. 11).

$$\min (OF) = \widehat{CSA} + \widehat{FS} + \widehat{SAR} + \widehat{RCP} \quad (9)$$

$$\text{s.t.} \quad RCP \geq 40 \text{ kPa} \quad (10) \quad t \leq 150 \mu\text{m} \quad (11)$$

241

242 3. Results

243 3.1 Baseline geometry

244 The baseline stent design parameters and the respective performance metrics are shown in Table 3.
245 Cross-sectional area (post-dilation) is difficult to measure *in vivo* and hence, there is limited
246 published data. However, the baseline design recoiled by approximately 9% following dilation, which
247 is comparable to commercial *PLLA BRS*.^[24] Given that the value of t is similar between the baseline
248 design and a commercial stent, by extension, the *CSA* will also be comparable. The baseline stent
249 design values for *SAR* and *FS* of 5.7% and 35.5%, respectively, are comparable to the upper end of
250 the commercial *PLLA BRS* range.^[12,24] However, the baseline stent value for *RCP* of 20.9 kPa is
251 approximately half of the minimum allowable collapse pressure for a coronary stent,^[18] thereby
252 justifying the requirement for the present optimisation study.

253 **Table 3.** Baseline stent design parameters (A_r , w , t , and l) and its respective performance metrics
254 (*CSA*, *FS*, *SAR*, and *RCP*).

A_r (-)	w (μm)	t (μm)	l (μm)	<i>CSA</i> (mm^2)	<i>FS</i> (%)	<i>SAR</i> (%)	<i>RCP</i> (kPa)
1.35	150	150	1050	-8.0	5.7	35.3	-20.9

255

256 3.2 Response surface methodology

257 The four performance metrics (*CSA*, *FS*, *SAR* and *RCP*) were computed for each of the 40 design
258 points (Table 4).

259 **Table 4.** Design parameters (A_r , w , t and l) and respective performance metrics (CSA , FS , SAR and
 260 RCP) for each point considered under the optimised Latin hypercube sampling plan.

<i>Design</i>	A_r (-)	w (μm)	t (μm)	l (μm)	CSA (mm^2)	FS (%)	SAR (%)	RCP (kPa)
1	0.90	101	191	1166	-6.2	3.4	26.7	-6.8
2	0.47	134	161	1001	-8.1	6.8	30.9	-18.9
3	0.52	119	154	1144	-7.0	4.2	30.5	-8.5
4	0.71	124	134	1039	-7.6	5.5	29.9	-13.1
5	2.23	146	169	1009	-8.4	5.8	33.6	-22.8
6	0.61	164	184	1016	-8.4	8.5	37.2	-35.3
7	0.57	179	156	956	-8.8	10.0	38.4	-39.9
8	1.90	189	189	1136	-8.4	6.4	45.5	-32.6
9	1.37	176	104	971	-9.2	7.4	38.3	-23.7
10	1.42	199	126	1084	-8.5	7.2	45.9	-27.7
11	1.94	151	121	1196	-8.1	3.6	39.1	-10.8
12	1.33	116	166	949	-8.1	6.6	26.3	-20.2
13	0.95	139	106	979	-8.6	6.6	31.4	-16.0
14	2.13	186	179	1046	-8.7	7.2	42.4	-36.8
15	1.80	169	146	994	-8.7	6.8	37.6	-29.4
16	1.23	161	176	904	-9.0	9.5	33.8	-45.3
17	1.52	129	144	1189	-6.9	3.1	33.7	-8.8
18	1.61	191	174	941	-9.1	9.5	40.1	-53.9
19	2.04	136	136	964	-8.4	5.8	30.6	-18.1
20	2.18	156	141	1076	-8.9	5.1	37.2	-18.6
21	1.09	194	111	911	-9.0	10.5	39.6	-35.0
22	1.18	141	124	1091	-8.2	4.7	34.4	-13.8
23	2.28	154	164	1174	-7.8	4.1	39.1	-14.5
24	1.28	196	196	1024	-8.8	9.1	43.5	-51.0
25	1.04	184	139	1114	-8.2	6.6	43.9	-24.7
26	1.99	126	114	1054	-7.7	3.9	30.4	-10.5
27	1.47	104	159	1069	-7.0	3.8	25.7	-9.2
28	1.56	131	199	1061	-7.8	4.9	31.6	-20.4
29	2.09	109	151	986	-7.8	4.9	25.4	-12.4
30	0.76	181	109	1129	-8.0	6.7	43.8	-17.4
31	1.75	149	194	934	-8.8	8.0	32.3	-38.0
32	0.66	171	129	919	-8.8	9.7	36.0	-31.6
33	0.99	106	116	926	-7.8	6.1	23.9	-12.9
34	0.42	159	131	1031	-8.9	7.5	36.6	-18.6
35	1.66	114	119	1121	-6.9	3.2	28.9	-6.9
36	1.85	111	186	1151	-6.8	3.2	28.9	-8.7
37	0.80	144	149	1181	-7.2	4.6	37.0	-12.1
38	1.71	166	101	1106	-8.5	5.0	40.1	-14.3
39	0.85	121	171	1099	-7.2	4.7	30.2	-12.7
40	1.14	174	181	1159	-7.9	5.9	43.1	-25.7

261 Multiple linear regression analysis (Table 5) was performed to generate constitutive equations that
 262 related each performance metric to the input parameters. A second-order model containing the
 263 intercept, main factors, two-factor interactions and quadratic terms (Eq. 12) was used for *CSA*, *FS*,
 264 *SAR* and *RCP*. Using the constants in Table 5, each model predicted, with approximately 99.7%
 265 confidence, that all values lie within the mean prediction plus or minus three standard deviations
 266 (Fig. 7). Model quality is assessed in Fig. 8, in which the performance metrics were predicted for a
 267 given set of design parameters using the statistical model (Eq. 12), and compared to their
 268 corresponding actual (measured) values extracted from finite element simulations. Linear behaviour
 269 was observed for *CSA*, *FS*, *SAR* and *RCP*, with the statistical models achieving R-squared (R^2) values of
 270 0.950, 0.996, 0.999 and 0.996, respectively.

$$Y = \beta_0 + \beta_1 A_r + \beta_2 w + \beta_3 t + \beta_4 l + \beta_5 A_r w + \beta_6 A_r t + \beta_7 A_r l + \beta_8 w t + \beta_9 w l + \beta_{10} t l + \beta_{11} A_r^2 + \beta_{12} w^2 + \beta_{13} t^2 + \beta_{14} l^2 \quad (12)$$

271 where Y denotes the predicted response for a given performance metric, i.e. *CSA*, *FS*, *SAR* and *RCP*.

272 **Table 5.** Statistical model coefficients for *CSA*, *FS*, *SAR* and *RCP*.

	CSA	FS	SAR	RCP
Intercept	-2.6	44.9	-1.1	-25.3
A_r	16.0E-1	-26.6E-1	-4.7E-1	-69.2E-1
w	-55.7E-3	6.6E-3	96.3E-3	-249.7E-3
t	-2.7E-3	25.3E-3	1.5E-3	-422.3E-3
l	-7.1E-3	-67.5E-3	3.1E-3	110.3E-3
$A_r:w$	-3.8E-3	-6.8E-3	1.5E-3	-2.0E-3
$A_r:t$	7.1E-4	10.4E-4	3.3E-4	183.6E-4
$A_r:l$	-10.6E-4	11.6E-4	1.7E-4	-16.0E-4
$w:t$	2.6E-5	2.6E-5	-1.1E-5	-225.7E-5
$w:l$	-2.3E-5	-1.2E-5	15.9E-5	56.3E-5
$t:l$	9.8E-6	-35.7E-6	-4.2E-6	612.6E-6
A_r^2	-7.5E-2	48.5E-2	1.3E-2	251.7E-2
w^2	2.2E-4	1.8E-4	-2.0E-4	-9.3E-4
t^2	-3.6E-5	5.8E-5	1.2E-5	-22.5E-5
l^2	7.3E-6	27.9E-6	-1.3E-6	-104.5E-6

273

274 **Fig. 7.** Standardised residual vs. predicted response using the statistical model in Eq. *Error! Reference*

275 *source* *not* *found.* for

276 (a) *CSA*; (b) *FS*; (c) *SAR* and (d) *RCP*.

277

278 **Fig. 8.** Predicted response using the statistical model in Eq. *Error! Reference source not found.* vs. actual

279 (measured) response from finite element simulations for (a) *CSA*; (b) *FS*; (c) *SAR* and (d) *RCP*.

280 A comparison of absolute t-values (for coefficients) from multiple regression analyses for each

281 performance metric is shown in Fig. 9a–d. Main factors, two-factor interactions and quadratic terms

282 are considered statistically significant ($p < 0.05$) if their absolute t-value lies above the dashed line.

283

284 **Fig. 9.** Comparison of absolute t-values (for coefficients) from multiple regression analyses

285 highlighting significant ($p < 0.05$) main factors and two-way interactions for (a) *CSA*; (b) *FS*; (c) *SAR*

286 and (d) *RCP*.

287 Response surfaces were plotted for all two-way interactions (Fig. 10), which highlight the combined

288 influence of any two design parameters (A_r , w , t or l) on each performance metric (*CSA*, *FS*, *SAR* and

289 *RCP*). For each response surface, the performance metric was plotted against two dependent design

290 parameters whilst the remaining two independent parameters were held constant at their baseline

291 (midpoint) value. For each response surface, moving from the purple region to the yellow region

292 indicates an improvement.

293

294 **Fig. 10.** Response surfaces highlighting the combined influence of any two design parameters

295 (A_r , w , t or l) on each performance metric (*CSA*, *FS*, *SAR* and *RCP*). For each response surface, the

296 remaining two (independent) design parameters are held constant at their baseline value.

297 The Pareto fronts (Fig. 11) highlight the trade-offs between each set of performance metrics, with
298 better designs lying towards the bottom left corner. Trade-offs were observed for *CSA* vs. *FS*,
299 *CSA* vs. *SAR*, *FS* vs. *RCP* and *SAR* vs. *RCP*, whilst no trade-offs were observed for *CSA* vs. *RCP* or *FS* vs.
300 *SAR*. Trade-offs occurred as a result of conflicting requirements for stent design, i.e. geometric
301 and/or material parameters that improve one metric often negatively affect at least one of the other
302 metrics.

303

304 **Fig. 11.** Trade-off curves for all permutations of the four performance metrics: (a) *CSA* vs. *FS*;
305 (b) *CSA* vs. *SAR*, (c) *CSA* vs. *RCP* and (d) *FS* vs. *SAR*, (e) *FS* vs. *RCP* and (f) *SAR* vs. *RCP*.

306 3.3 Optimisation

307 To construct a single dimensionless objective function, each performance metric was normalised
308 (scaled) to the same range [0,1] based on its minimum and maximum attainable values (Table 6),
309 attained using least squares minimisation (Eq. 13).

310 **Table 6.** Minimum and maximum values for each performance metric (*CSA*, *FS*, *SAR* and *RCP*).

	<i>CSA</i> (mm ²)	<i>FS</i> (%)	<i>SAR</i> (%)	<i>RCP</i> (kPa)
Min.	-9.4	2.3	22.1	-72.6
Max.	-5.8	13.9	50.0	-0.7

311

$$\hat{Y} = \frac{Y - Y_{min}}{Y_{max} - Y_{min}} \quad (13)$$

312 where \hat{Y} and Y denote the predicted normalised and absolute responses, respectively, for a given
313 performance metric, whilst Y_{min} and Y_{max} denote the minimum and maximum attainable values.

314 Multi-objective optimisation produced a stent design superior to the baseline with $t = 150 \mu\text{m}$ and
315 $w = 173 \mu\text{m}$ (Table 7), which are lower than some commercial polymeric stents,^[12] whilst meeting
316 the minimum allowable collapse pressure.^[18] A comparison between the baseline design and the

317 optimised design is shown in Fig. 12, in which each performance metric has been normalised. The
318 *RCP* of the optimal design is approximately twice that of the baseline design with a less than 1%
319 increase in *SAR*. The *CSA* increased by 14% and whilst *FS* increased, a value of 8% is comparable to
320 stents in commercial use.^[51]

321 **Table 7.** Comparison between baseline (base.) and optimal (opt.) stent designs highlighting design
322 parameters and their respective performance metrics.

	<i>A_r</i> (-)	<i>w</i> (μm)	<i>t</i> (μm)	<i>l</i> (μm)	<i>CSA</i> (mm^2)	<i>FS</i> (%)	<i>SAR</i> (%)	<i>RCP</i> (kPa)
Base.	1.35	150	150	1050	-8	5.7	35.3	-20.9
Opt.	2.3	173	150	900	-9.1	8	35.7	-40

323

324

325 **Fig. 12.** Visual comparison of normalised performance metrics and design parameters between the
326 baseline design and the optimal design.

327 4. Discussion

328 This study proposes a multi-objective optimisation framework that considers the combined effect of
329 the biaxial stretching processing history and the geometric configuration when optimising the short-
330 term (pre-degradation) mechanical performance of a *PLLA* coronary stent. Given that the ideal stent
331 must fulfil a range of conflicting technical requirements, a multi-objective optimisation process that
332 offers compromises between key performance metrics was conducted to develop a polymeric stent
333 that offered improved performance relative to a baseline design for the same strut thickness
334 (150 μm). Performance trade-offs were observed (Fig. 11) and may be explained using the absolute
335 t-value comparisons for coefficients (Fig. 9a–d) and the response surface interaction plots for each
336 performance metric (Fig. 10). The absolute t-value comparisons for coefficients highlight statistically
337 significant ($p < 0.05$) factors for each performance metric whilst the response surface interaction
338 plots provide a visual aid in understanding the interdependent effect between two factors on a given
339 performance metric.

340 4.1 Cross-sectional area vs. foreshortening

341 The trade-off between *CSA* and *FS* was primarily due to the conflicting requirements for w and l .
342 Cross-sectional area was most strongly affected by w and w^2 (Fig. 9a), whilst *FS* was most strongly
343 affected by l and l^2 (Fig. 9b). Increasing w improved *CSA* as a wider strut increased plastic
344 deformation in the hoops and reduced radial recoil, which is in agreement with the findings of Pant
345 et al.^[40] Furthermore, the presence of a significant ($p < 0.05$) quadratic effect (w^2) in the model
346 suggested a curvilinear relationship between *CSA* and w . This was evident from the interaction plots
347 in which w was plotted as one of the dependent variables (Fig. 10). A convex relationship was
348 observed between *CSA* and w , i.e. *CSA* improved as w increased but with diminishing returns.
349 Decreasing l further improved *CSA* and was evident from the interaction plot between w and l . By
350 increasing w from 100 μm to 200 μm and decreasing l from 1,200 μm to 900 μm , *CSA* improved by
351 approximately 53%. However, this change caused an undesirable increase in *FS* from 3% to 11%. In

352 contrast to the requirements for *CSA*, narrow, long struts were ideal for reducing *FS*, as the struts
353 deformed less to achieve an equivalent level of plastic strain, thereby reducing the level of axial
354 contraction. This is in agreement with Li et al.^[39] who acknowledged the contrasting requirements
355 for *l*, based on the observed trade-off between recoil and *FS*. Strut thickness has the weakest effect
356 on *CSA* — whilst a higher value of *t* reduced the degree of radial recoil post-inflation, it was not
357 offset by the reduced *CSA* (as a result of the thicker struts) pre-inflation. In general, it was beneficial
358 to design the stent such that it is stiffer in the circumferential direction (higher A_r) as *FS* improved
359 without negatively affecting *CSA*. Hence, a lower value of *l* and A_r were desirable.

360 **4.2 Cross-sectional area vs. stent-to-artery ratio**

361 The trade-off between *CSA* and *SAR* was primarily due to the conflicting requirements for *w*.
362 Although high values of *w* improved *CSA*, a wider strut increased the surface area of the stent which
363 negatively affects *SAR*. Low values of *l* were correlated with improved *CSA*, and were also correlated
364 with improved *SAR* as, intuitively, a shorter strut reduced the surface area of the stent. The
365 interaction between *w* and *l* had the strongest effect on *SAR* (Fig. 9c) and was evident from the
366 response surface plot (Fig. 10). Stent-to-artery ratio was unaffected by *t* and A_r and hence, it was
367 beneficial to design the stent with high values of A_r and *t* as these parameters improved *CSA*. High
368 values of A_r and *t*, combined with a low value of *l* are ideal for improving both *CSA* and *SAR*. By
369 holding each of these design parameters constant at their optimal limits and increasing *w* from 100
370 μm to 200 μm , *CSA* improved by approximately 20%. However, *SAR* had an undesirable increase
371 from 22% to 40%, which is significantly higher than the *SAR* for both polymer and metallic stents in
372 clinical practice, and may contribute to increased levels of thrombosis.^[12,13]

373 **4.3 Foreshortening vs. radial collapse pressure**

374 The trade-off between *FS* and *RCP* was primarily due to the conflicting requirements for *w*, *t* and *l*.
375 Radial collapse pressure was most strongly affected by the interactions between *w* and *t*, *w* and *l*
376 and *t* and *l*, with each interaction considered statistically significant ($p < 0.05$) (Fig. 9d). The response

377 surface plots for each of these interactions (Fig. 10) showed that *RCP* improves with high values of *t*
378 and *w*, combined with low values of *l*. This combination of parameters tended to induce higher levels
379 of plastic deformation in the strut hoops. By increasing *w* and *t* from 100 μm to 200 μm and
380 decreasing *l* from 1,200 μm to 900 μm , *RCP* improved from 8.8 kPa to 70 kPa, meeting the minimum
381 allowable collapse pressure of 40 kPa.^[18] However, this change caused an undesirable increase in *FS*
382 from 2.5% to 12%. In general, *A_r* did not strongly affect *RCP* and was not considered statistically
383 significant ($p > 0.05$). However, given that a higher *A_r* improved *FS*, it was beneficial to design the
384 stent such that it is stiffer in the circumferential direction.

385 **4.4 Stent-to-artery ratio vs. radial collapse pressure**

386 The trade-off between *SAR* and *RCP* is similar to the trade-off observed between *SAR* and *CSA*, and is
387 primarily due to the conflicting requirements for *w*. High values of *A_r* and *t*, combined with a low
388 value of *l* are ideal for improving both *RCP* and *SAR*. By holding each of these design parameters
389 constant at their optimal limits and increasing *w* from 100 μm to 200 μm , *RCP* had a more than
390 three-fold increase. However, *SAR* had an undesirable increase of approximately 80%.

391 **4.5 Limitations**

392 In this study, stent geometries were based on a conventional open-cell design with straight bridges,
393 which has proved ideal for metallic drug-eluting stents. However, this does not guarantee
394 compatibility when using a polymer such as *PLLA* as the platform material, given that it exhibits an
395 entirely different stress-strain response. Modifying the bridge geometry, strut cross-section and
396 hinge profile have all been shown to influence the mechanical performance of stents^[40,52] and the
397 inclusion of these parameters may permit the evaluation of unconventional (or unorthodox)
398 geometries that are better suited to polymeric stents. In addition to increasing the number of design
399 parameters, the inclusion of a stenosed artery into the finite element model would permit additional
400 performance metrics to be evaluated. Modelling the expansion of a stent in a stenosed artery could
401 provide an indication of high risk areas in the stented region and may also be used to evaluate the

402 stent's susceptibility to fracture. However, increasing the number of design parameters and
403 performance metrics will increase the computational cost and complexity of the optimisation. Given
404 that the performance metrics and design parameters evaluated within the present study were
405 considered most critical based on the literature reviewed, any alternatives should be evaluated as
406 additions rather than replacements. Finally, there is limited information in literature on clinically
407 acceptable values for performance metrics such as foreshortening and stent-to-artery ratio.
408 Identification of operational limits for these metrics is essential, as these limits can be used as
409 constraints for the multi-objective optimisation procedure to tailor stent designs for a particular
410 lesion or patient geometry, suggesting an area for future research.

411 **5. Conclusion**

412 An optimisation framework has been proposed that considers the combined effect of the biaxial
413 stretching processing history and the geometric configuration when optimising the mechanical
414 performance of a *PLLA* coronary stent. Response surface methodology combined with multi-
415 objective optimisation produced an optimal *PLLA* stent design that offered improved performance
416 relative to a baseline design for the same strut thickness (150 μm). The effects of each of the design
417 parameters (A_r , w , t and l) on individual performance metrics (CSA , FS , SAR and RCP) have been
418 quantified and compared. For each of the design parameters, a main factor or two-way interactions
419 term had a statistically significant ($p < 0.05$) effect on at least one of the performance metrics.
420 Pareto fronts highlighted that a change in one design parameter that improves one metric often
421 leads to a compromise in at least one of the other metrics with trade-offs observed for CSA vs. FS ,
422 CSA vs. SAR , FS vs. RCP and SAR vs. RCP . In summary, this study addresses key limitations in
423 polymeric stent design and the methodology that could be applied in the development of high
424 stiffness, thin strut polymeric stents that contend with the performance of their metallic
425 counterparts.

426 **Conflict of interest**

427 There is no conflict of interest to be declared by the authors.

428 **Acknowledgements**

429 The authors wish to acknowledge funding from the Engineering and Physical Sciences Research
430 Council (EPSRC) (S3804ASA) and the Marie Skłodowska-Curie Research and Innovation Staff
431 Exchange (RISE), grant agreement 691238. The authors also wish to acknowledge the research
432 institutions involved in the Bi-Stretch-4-Biomed collaborative RISE project (California Institute of
433 Technology, University of Warwick and ENEA: Italian National Agency for New Technologies, Energy
434 and Sustainable Economic Development).

435 References

- 436 1. **Grüntzig, A.**, 1978. Transluminal dilatation of coronary-artery stenosis. *The Lancet*,
437 **311**(8058):263.
- 438 2. **Sigwart, U., Puel, J., Mirkovitch, V., Joffre, F. and Kappenberger, L.**, 1987. Intravascular stents
439 to prevent occlusion and re-stenosis after transluminal angioplasty. *New England Journal of*
440 *Medicine*, **316**(12):701-706.
- 441 3. **Windecker, S., Mayer, I., De Pasquale, G., Maier, W., Dirsch, O., De Groot, P., Wu, Y. P., Noll,**
442 **G., Leskosek, B., Meier, B. and Hess, O. M.**, 2001. Stent coating with titanium-nitride-oxide for
443 reduction of neointimal hyperplasia. *Circulation*, **104**(8):928–933.
- 444 4. **Iqbal, J., Onuma, Y., Ormiston, J., Abizaid, A., Waksman, R. and Serruys, P.**, 2013. Bioresorbable
445 scaffolds: rationale, current status, challenges, and future. *European Heart Journal*, **35**(12):765–
446 776.
- 447 5. **Morice, M. C., Serruys, P. W., Sousa, J. E., Fajadet, J., Ban Hayashi, E., Perin, M., Colombo, A.,**
448 **Schuler, G., Barragan, P., Guagliumi, G. and Molnar, F.**, 2002. A randomized comparison of a
449 sirolimus-eluting stent with a standard stent for coronary revascularization. *New England Journal*
450 *of Medicine*, **346**(23):1773–1780.
- 451 6. **Stettler, C., Wandel, S., Allemann, S., Kastrati, A., Morice, M. C., Schömig, A., Pfisterer, M. E.,**
452 **Stone, G. W., Leon, M. B., de Lezo, J. S. and Goy, J. J.**, 2007. Outcomes associated with drug-
453 eluting and bare-metal stents: a collaborative network meta-analysis. *The Lancet*,
454 **370**(9591):937-948.
- 455 7. **Bavry, A. A., Kumbhani, D. J., Helton, T. J., Borek, P. P., Mood, G. R. and Bhatt, D. L.**, 2006. Late
456 thrombosis of drug-eluting stents: a meta-analysis of randomized clinical trials. *The American*
457 *Journal of Medicine*, **119**(12):1056–1061.
- 458 8. **Kang, S.H., Chae, I.H., Park, J.J., Lee, H.S., Kang, D.Y., Hwang, S.S., Youn, T.J. and Kim, H.S.**,
459 2016. Stent thrombosis with drug-eluting stents and bioresorbable scaffolds: evidence from a
460 network meta-analysis of 147 trials. *JACC: Cardiovascular Interventions*, **9**(12):1203–1212.
- 461 9. **van Beusekom, H. M., Saia, F., Zindler, J. D., Lemos, P. A., Hoor, S. L. S. T., van Leeuwen, M. A.,**
462 **Feijter, P. J., Serruys, P. W. and van der Giessen, W. J.**, 2007. Drug-eluting stents show delayed
463 healing: paclitaxel more pronounced than sirolimus. *European Heart Journal*, **28**(8):974–979.

- 464 **10. Gomez-Lara, J., Garcia-Garcia, H. M., Onuma, Y., Garg, S., Regar, E., De Bruyne, B., Windecker,**
465 **S., McClean, D., Thuesen, L., Dudek, D. and Koolen, J., 2010.** A comparison of the conformability
466 of everolimus-eluting bioresorbable vascular scaffolds to metal platform coronary stents. *JACC:*
467 *Cardiovascular Interventions*, **3**(11):1190–1198.
- 468 **11. Serruys, P. W., Garcia-Garcia, H. M. and Onuma, Y., 2011.** From metallic cages to transient
469 bioresorbable scaffolds: change in paradigm of coronary revascularization in the upcoming
470 decade? *European Heart Journal*, **33**(1):16–25.
- 471 **12. Kawamoto, H., Jabbour, R. J., Tanaka, A., Latib, A. and Colombo, A., 2016.** The bioresorbable
472 scaffold: will oversizing affect outcomes? *JACC: Cardiovascular Interventions*, **9**(3):299–300.
- 473 **13. Kolandaivelu, K., Swaminathan, R., Gibson, W. J., Kolachalama, V. B., Nguyen-Ehrenreich, K. L.,**
474 **Giddings, V. L., Coleman, L., Wong, G. K. and Edelman, E. R., 2011.** Stent Thrombogenicity Early
475 in High-Risk Interventional Settings Is Driven by Stent Design and Deployment and Protected by
476 Polymer-Drug Coatings. *Circulation*, **123**(13):1400–1409.
- 477 **14. Kastrati, A., Mehilli, J., Dirschinger, J., Dotzer, F., Schühlen, H., Neumann, F. J., Fleckenstein, M.**
478 **D., Pfafferott, M. D., Seyfarth, M. and Schömig, A., 2001.** Intracoronary stenting and
479 angiographic results: strut thickness effect on restenosis outcome (ISAR-STEREO) trial.
480 *Circulation*, **103**(23):2816–2821.
- 481 **15. Serruys, P. W., Chevalier, B., Sotomi, Y., Cequier, A., Carrié, D., Piek, J. J., and Helqvist, S., 2016.**
482 Comparison of an everolimus-eluting bioresorbable scaffold with an everolimus-eluting metallic
483 stent for the treatment of coronary artery stenosis (ABSORB II): a 3 year, randomised,
484 controlled, single-blind, multicentre clinical trial. *The Lancet*, **388**(10059):2479–2491.
- 485 **16. Ako, J., Bonneau, H. N., Honda, Y. and Fitzgerald, P. J., 2007.** Design criteria for the ideal drug-
486 eluting stent. *The American Journal of Cardiology*, **100**(8):S3-S9.
- 487 **17. Lim, D., Cho, S. K., Park, W. P., Kristensson, A., Ko, J. Y., Al-Hassani, S. T. S. and Kim, H. S., 2008.**
488 Suggestion of potential stent design parameters to reduce restenosis risk driven by
489 foreshortening or dogboning due to non-uniform balloon-stent expansion. *Annals of Biomedical*
490 *Engineering*, **36**(7):1118–1129.
- 491 **18. Agrawal, C. M., Haas, K. F., Leopold, D. A. and Clark, H. G., 1992.** Evaluation of poly (L-lactic acid)
492 as a material for intravascular polymeric stents. *Biomaterials*, **13**(3):176–182.

- 493 **19. McMahon, S., Bertollo, N., O’Cearbhaill, E. D., Salber, J., Pierucci, L., Duffy, P. and Wang, W.,**
494 2018. Bio-resorbable polymer stents: a review of material progress and prospects. *Progress in*
495 *Polymer Science*, **83**:79–96.
- 496 **20. Pauck, R. G. and Reddy, B. D.,** 2015. Computational analysis of the radial mechanical
497 performance of PLLA coronary artery stents. *Medical Engineering and Physics*, **37**(1):7–12.
- 498 **21. Ang, H. Y., Bulluck, H., Wong, P., Venkatraman, S. S., Huang, Y. and Foin, N.,** 2017.
499 Bioresorbable stents: Current and upcoming bioresorbable technologies. *International Journal of*
500 *Cardiology*, **228**:931–939.
- 501 **22. Grogan, J. A., Leen, S. B. and McHugh, P. E.,** 2012. Comparing coronary stent material
502 performance on a common geometric platform through simulated bench testing. *Journal of the*
503 *Mechanical Behavior of Biomedical Materials*, **12**:129–138.
- 504 **23. Menown, I. B., Noad, R., Garcia, E. J. and Meredith, I.,** 2010. The platinum chromium element
505 stent platform: from alloy, to design, to clinical practice. *Advances in Therapy*, **27**(3):129–141.
- 506 **24. Schmidt, W., Behrens, P., Brandt-Wunderlich, C., Siewert, S., Grabow, N. and Schmitz, K. P.,**
507 2016. In vitro performance investigation of bioresorbable scaffolds—standard tests for vascular
508 stents and beyond. *Cardiovascular Revascularization Medicine*, **17**(6):375–383.
- 509 **25. Schmidt, W., Behrens, P. and Schmitz, K. P.,** 2009. Biomechanical aspects of potential stent
510 malapposition at coronary stent implantation. *Proceedings of the World Congress on Medical*
511 *Physics and Biomedical Engineering*, pages 136–139.
- 512 **26. Bobel, A. C., Petisco, S., Sarasua, J. R., Wang, W. and McHugh, P. E.,** 2015. Computational bench
513 testing to evaluate the short-term mechanical performance of a polymeric stent. *Cardiovascular*
514 *Engineering and Technology*, **6**(4):519–532.
- 515 **27. Bergström, J. S. and Hayman, D.,** 2015. An overview of mechanical properties and material
516 modeling of polylactide (PLA) for medical applications. *Annals of Biomedical Engineering*,
517 **44**(2):330–340.
- 518 **28. Alexy, R. D. and Levi, D. S.,** 2013. Materials and manufacturing technologies available for
519 production of a pediatric bioabsorbable stent. *BioMed Research International 2013*.
- 520 **29. Wu, J. H., Yen, M. S., Wu, C. P., Li, C. H. and Kuo, M. C.,** 2013. Effect of biaxial stretching on
521 thermal properties, shrinkage and mechanical properties of poly (lactic acid) films. *Journal of*
522 *Polymers and the Environment*, **21**(1):303–311.

- 523 **30. Blair, R. W., Dunne, N. J., Lennon, A. B. and Menary, G. H.,** 2018. Processing-property
524 relationships of biaxially stretched poly(L-lactic acid) sheet for application in coronary stents.
525 *Journal of the Mechanical Behavior of Biomedical Materials*, **86**:113–121.
- 526 **31. Bedoya, J., Meyer, C. A., Timmins, L. H., Moreno, M. R. and Moore, J. E.,** 2006. Effects of stent
527 design parameters on normal artery wall mechanics. *Journal of Biomechanical Engineering*,
528 **128**(5):757–765.
- 529 **32. Migliavacca, F., Petrini, L., Colombo, M., Auricchio, F. and Pietrabissa, R.,** 2002. Mechanical
530 behavior of coronary stents investigated through the finite element method. *Journal of*
531 *Biomechanics*, **35**(6):803–811.
- 532 **33. Pant, S., Limbert, G., Curzen, N. P. and Bressloff, N. W.,** 2011. Multiobjective design
533 optimisation of coronary stents. *Biomaterials*, **32**(31):7755–7773.
- 534 **34. Lally, C., Dolan, F. and Prendergast, P. J.,** 2005. Cardiovascular stent design and vessel stresses:
535 a finite element analysis. *Journal of biomechanics*, **38**(8):1574–1581.
- 536 **35. Bressloff, N. W., Ragkousis, G. and Curzen, N.,** 2016. Design optimisation of coronary artery
537 stent systems. *Annals of Biomedical Engineering*, **44**(2):357–367.
- 538 **36. Barragan, P., Rieu, R., Garitey, V., Roquebert, P. O., Sainsous, J., Silvestri, M. and Bayet, G.,**
539 2000. Elastic recoil of coronary stents: a comparative analysis. *Catheterization and*
540 *Cardiovascular Interventions*, **50**(1):112–119.
- 541 **37. Ota, T., Ishii, H., Sumi, T., Okada, T., Murakami, H., Suzuki, S., Kada, K., Tsuboi, N. and**
542 **Murohara, T.,** 2014. Impact of coronary stent designs on acute stent recoil. *Journal of*
543 *Cardiology*, **64**(5):347–352.
- 544 **38. García, A., Peña, E., and Martínez, M. A.,** 2012. Influence of geometrical parameters on radial
545 force during self-expanding stent deployment. Application for a variable radial stiffness stent.
546 *Journal of the Mechanical Behavior of Biomedical Materials*, **10**:166–175.
- 547 **39. Li, H., Wang, X., Wei, Y., Liu, T., Gu, J., Li, Z., Wang, M., Zhao, D., Qiao, A. and Liu, Y.,** 2017.
548 Multi-Objective Optimizations of Biodegradable Polymer Stent Structure and Stent
549 Microinjection Molding Process. *Polymers*, **9**(1):20.
- 550 **40. Pant, S., Bressloff, N. W., and Limbert, G.,** 2011. Geometry parameterization and
551 multidisciplinary constrained optimization of coronary stents. *Biomechanics and Modeling in*
552 *Mechanobiology*, **11**(1–2):61–82.

- 553 **41. Timmins, L. H., Moreno, M. R., Meyer, C. A., Criscione, J. C., Rachev, A. and Moore, J. E., 2007.**
554 Stented artery biomechanics and device design optimization. *Medical and Biological Engineering*
555 *and Computing*, **45**(5):505–513.
- 556 **42. Bobel, A. C. and McHugh, P. E., 2018.** Computational Analysis of the Utilisation of the Shape
557 Memory Effect and Balloon Expansion in Fully Polymeric Stent Deployment. *Cardiovascular*
558 *Engineering and Technology*, **9**(1):60–72.
- 559 **43. Blair, R. W., Dunne, N. J., Lennon, A. B. and Menary, G. H.** Characterisation and constitutive
560 modelling of biaxially stretched poly(L-lactic acid) sheet for application in coronary stents.
561 *Journal of the Mechanical Behavior of Biomedical Materials*, **97**:346–354.
- 562 **44. Bobel, A. C., Lohfeld, S., Shirazi, R. N. and McHugh, P. E., 2016.** Experimental mechanical testing
563 of Poly (l-Lactide) (PLLA) to facilitate pre-degradation characteristics for application in
564 cardiovascular stenting. *Polymer Testing*, **54**:150–158.
- 565 **45. Abbott,** 2012. Absorb Bioresorbable Vascular Scaffold System, Abbott Vascular, 3200 Lakeside
566 Drive, Santa Clara, CA 95054-2807, USA.
- 567 **46. Morris, M. D., Mitchell, T. J., 1995.** Exploratory designs for computational experiments. *Journal*
568 *of Statistical Planning and Inference*, **43**:381–402.
- 569 **47. R Core Team,** 2017. *R: A Language and Environment for Statistical Computing*, R Foundation for
570 *Statistical Computing*, Vienna, Austria. Retrieved from: <https://www.r-project.org/> [Accessed 19
571 Feb. 2018].
- 572 **48. Hunter, J. D., 2007.** Matplotlib: A 2D Graphics Environment, *Computing in Science & Engineering*,
573 **9**:90–95.
- 574 **49. Oliphant, T. E,** 2006. *A guide to NumPy*, USA: Trelgol Publishing. Retrieved from:
575 <http://www.numpy.org> [Accessed 5 Dec. 2018].
- 576 **50. Jones E., Oliphant E. and Peterson P., 2001.** *SciPy: Open Source Scientific Tools for Python*.
577 Retrieved from: <http://www.scipy.org/> [Accessed 6 Feb. 2019].
- 578 **51. Wang, W. Q., Liang, D. K., Yang, D. Z. and Qi, M., 2006.** Analysis of the transient expansion
579 behavior and design optimization of coronary stents by finite element method. *Journal of*
580 *Biomechanics*, **39**(1):21–32.

581 **52. Grogan, J. A., Leen, S.B. and McHugh, P. E., 2013. Optimizing the design of a bioabsorbable**
582 **metal stent using computer simulation methods. *Biomaterials*, 34(33):8049–8060.**

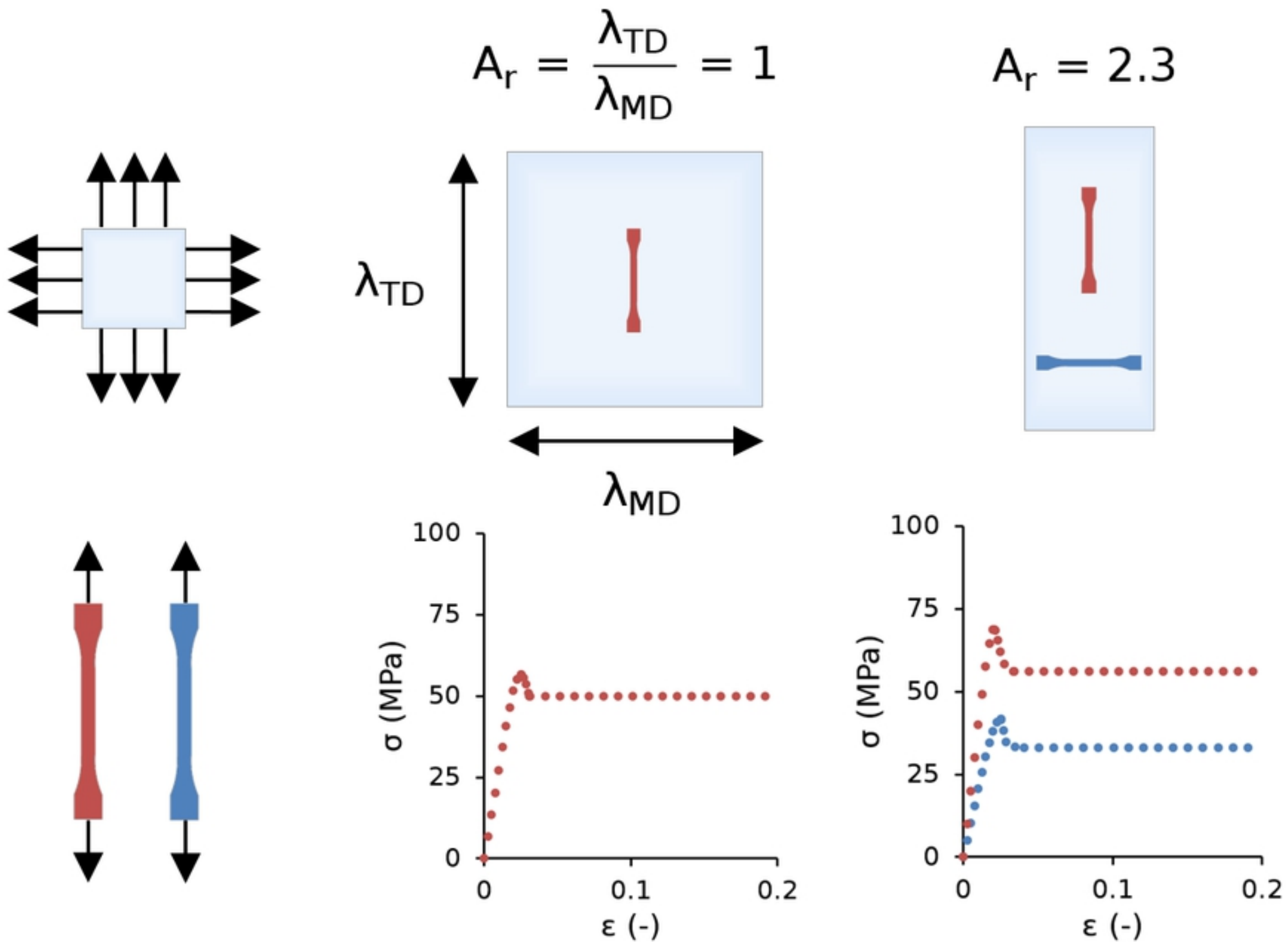


Figure 1

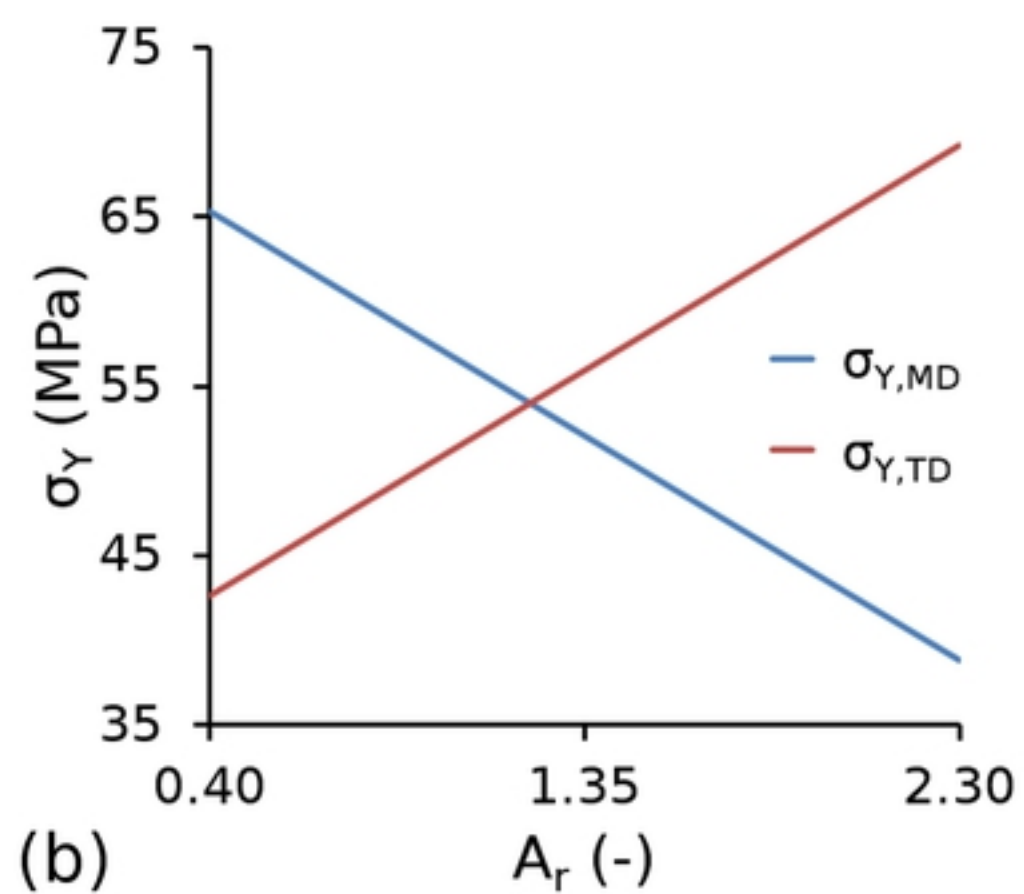
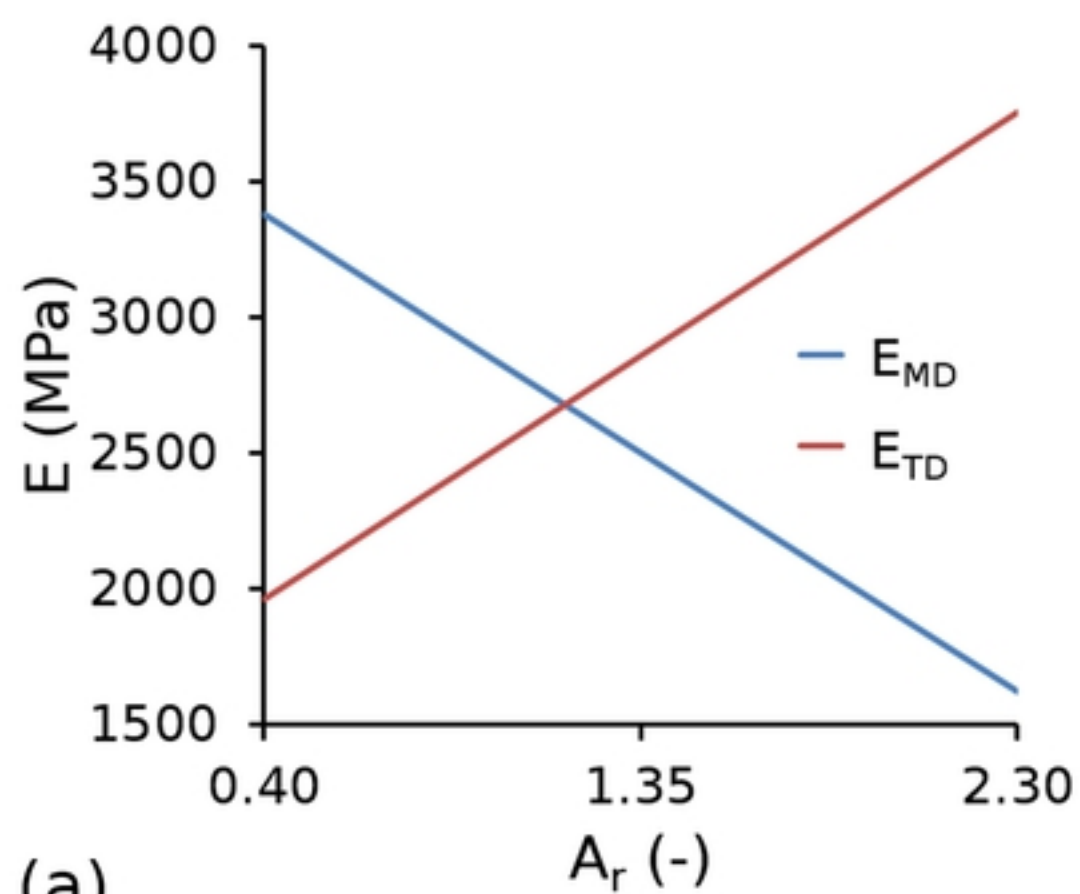


Figure 2

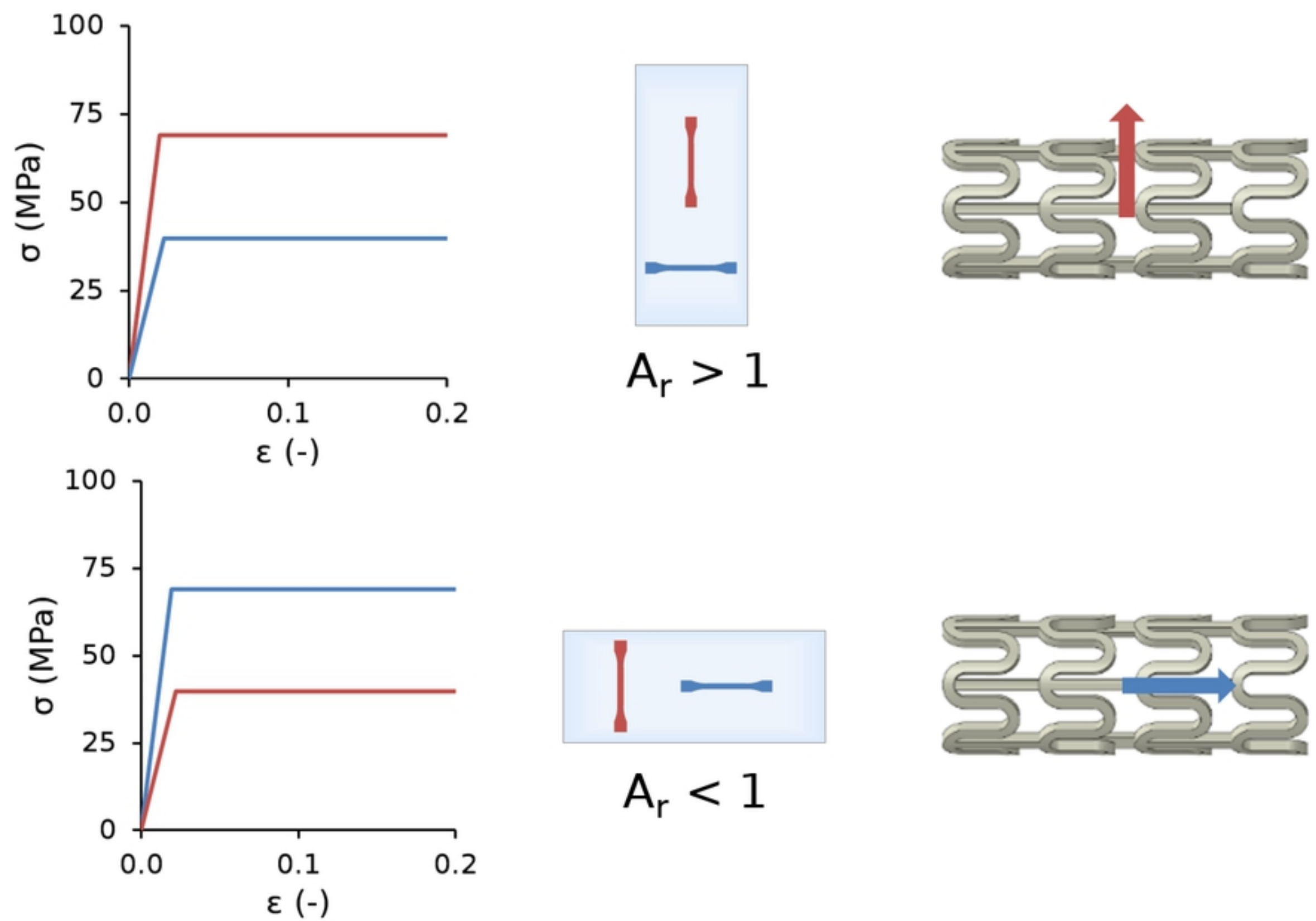


Figure 3

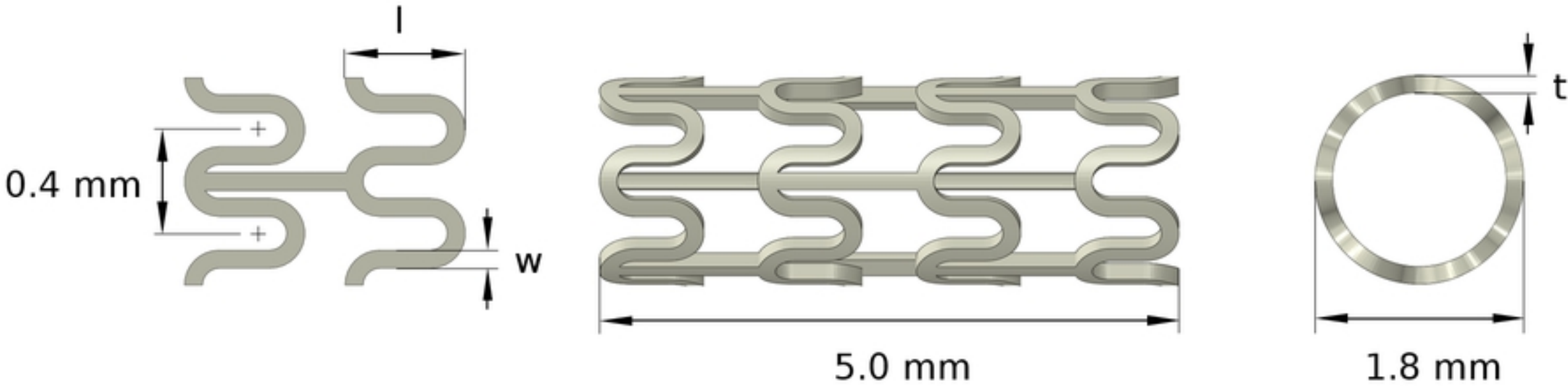
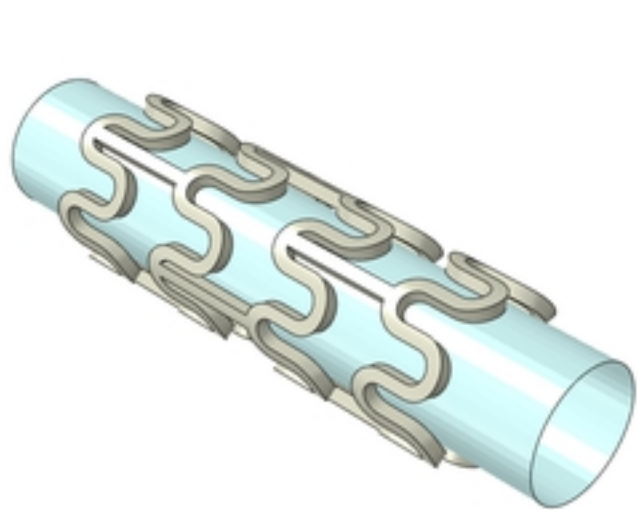
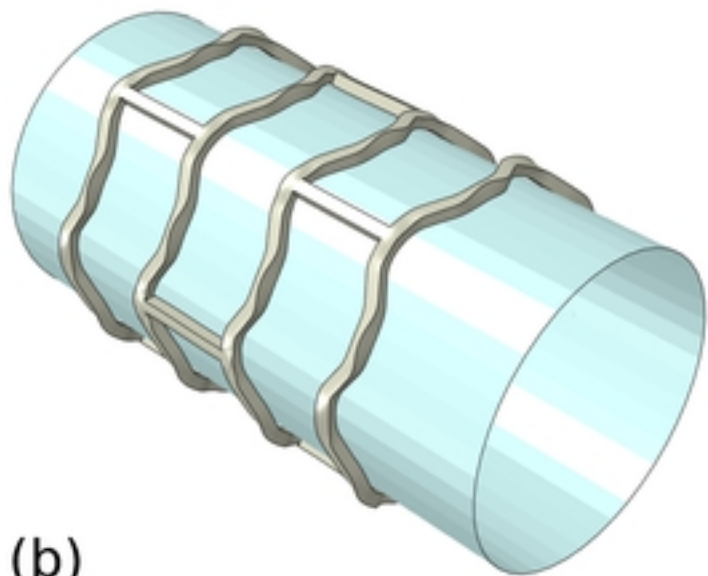


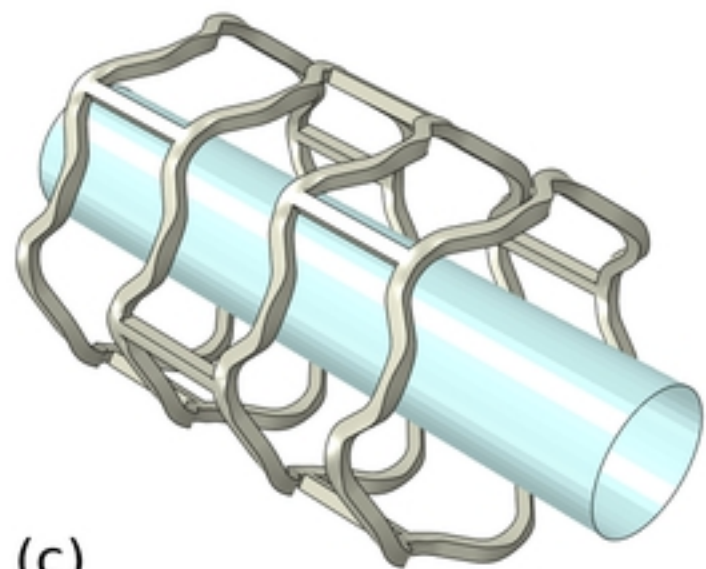
Figure 4



(a)

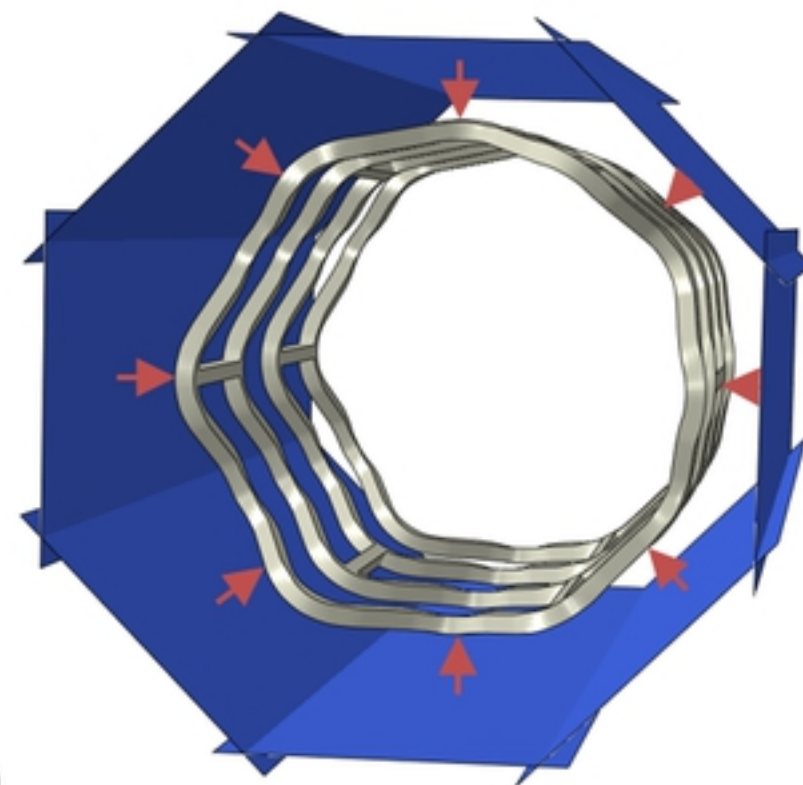
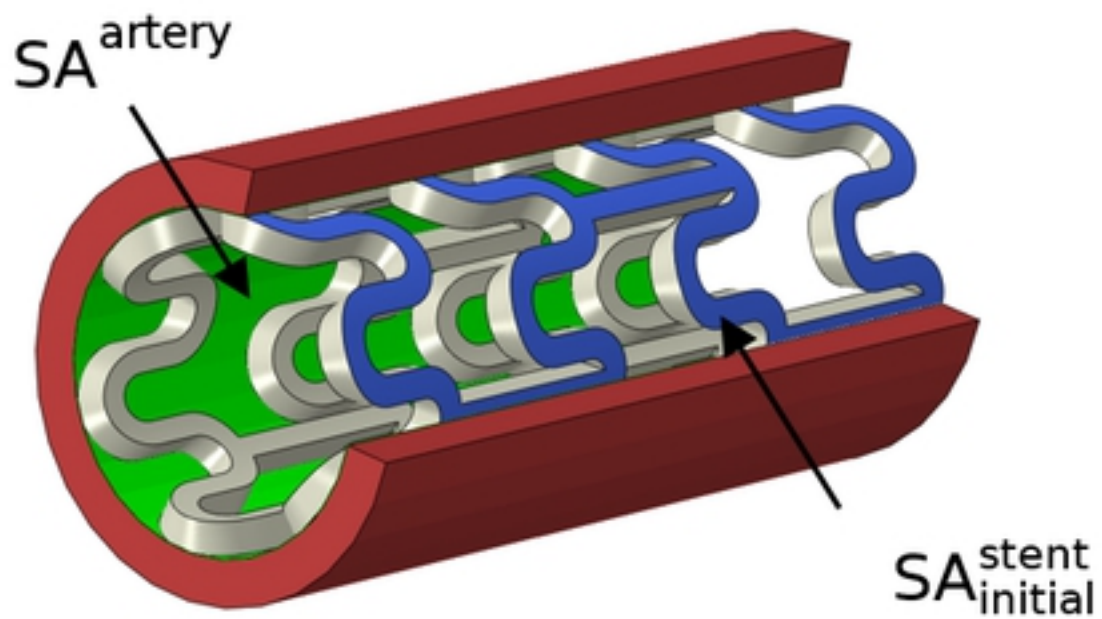
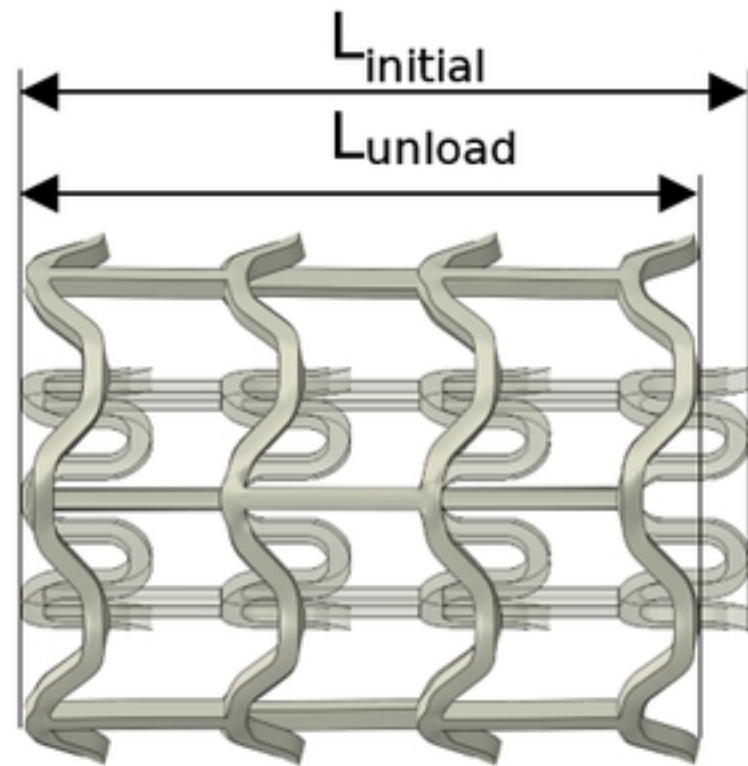
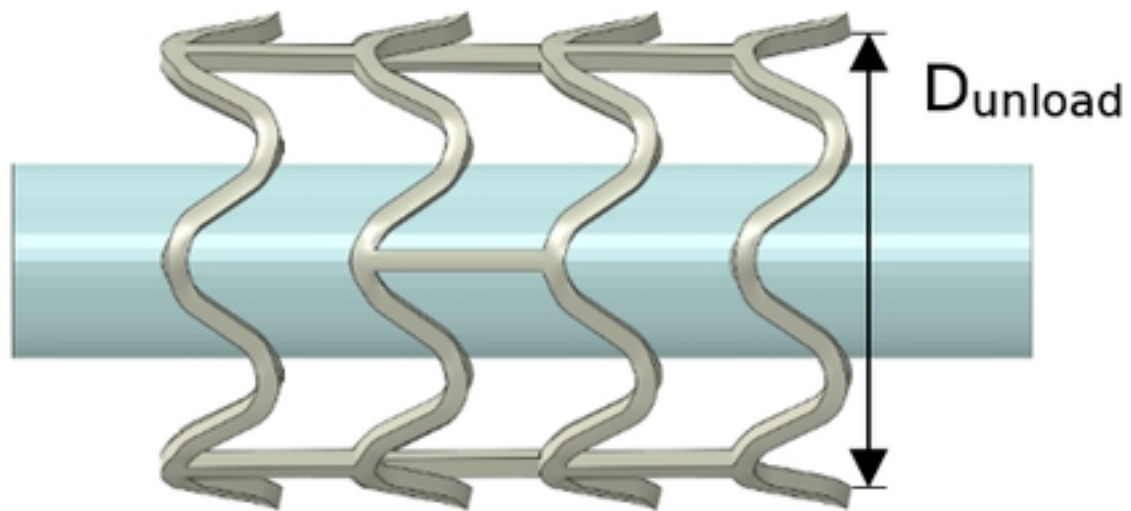


(b)



(c)

Figure 5



(a)
(b)
(c)
(d)
Figure 6



Figure 7

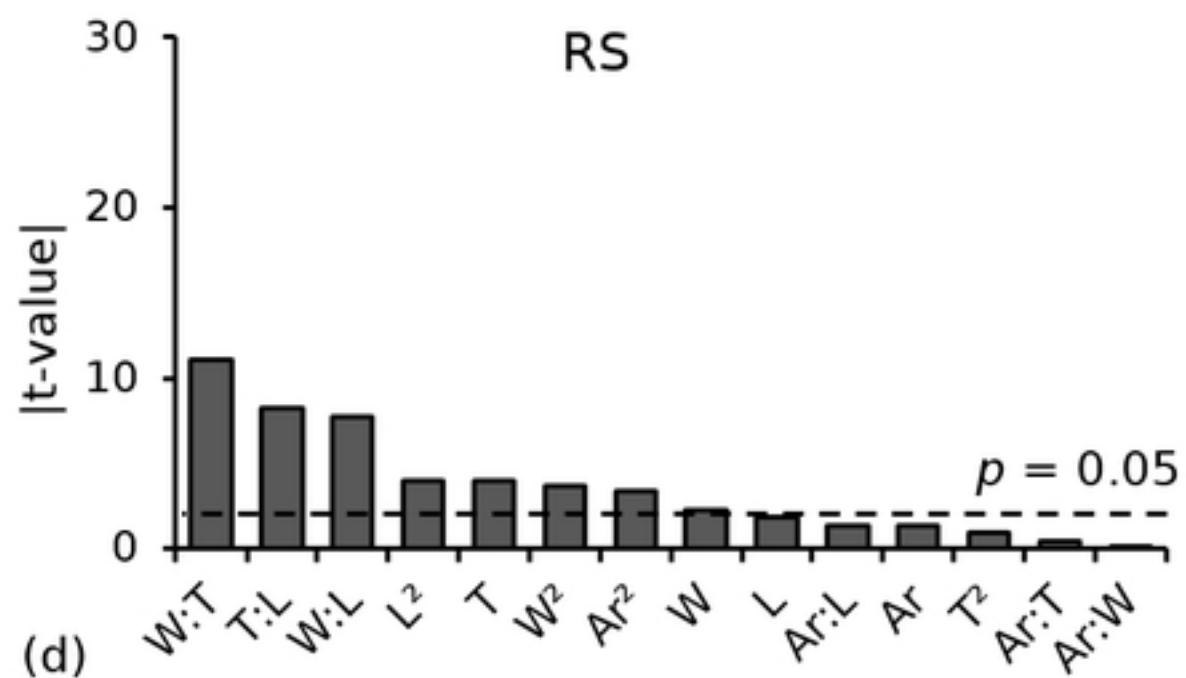
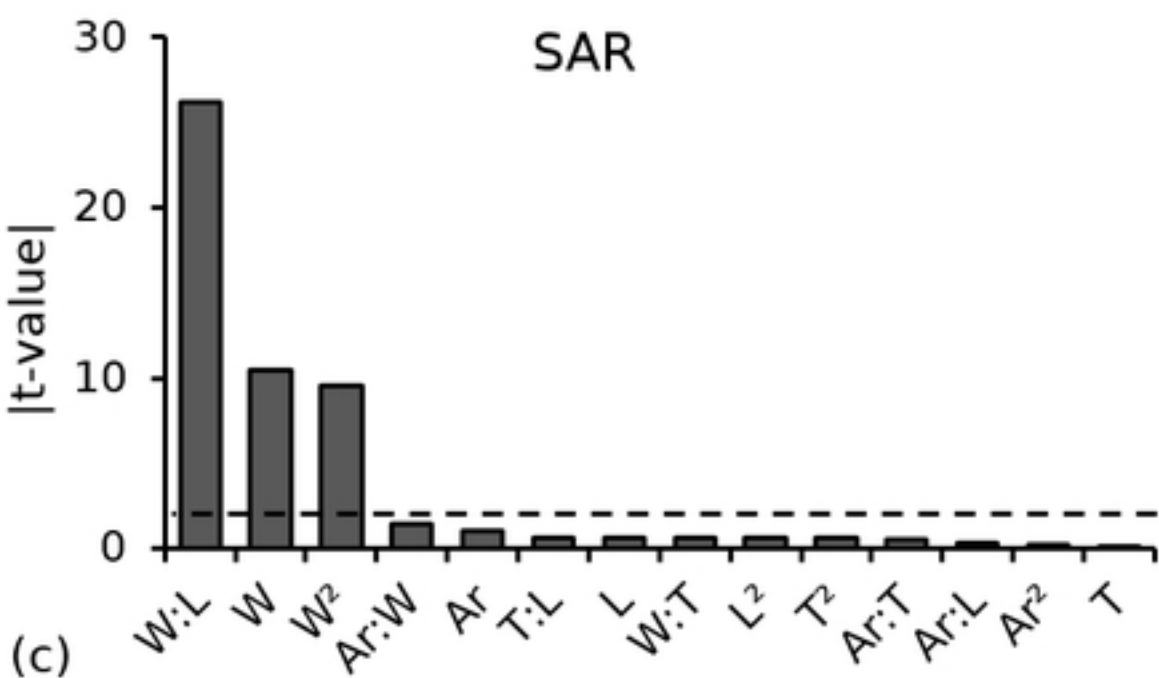
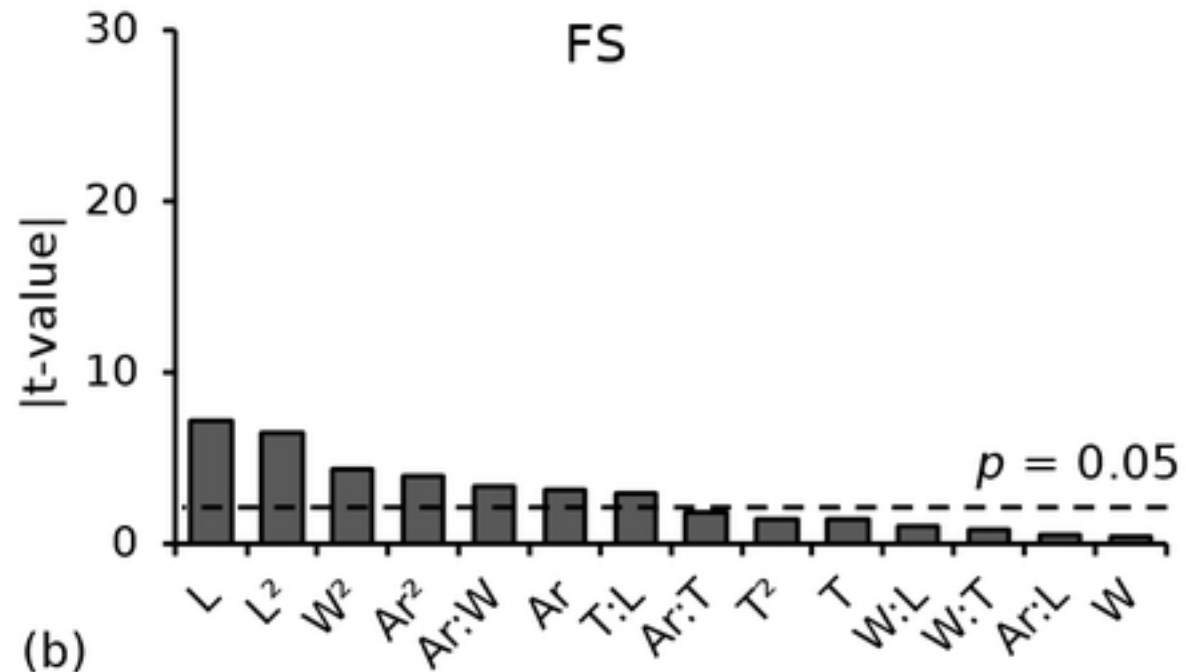
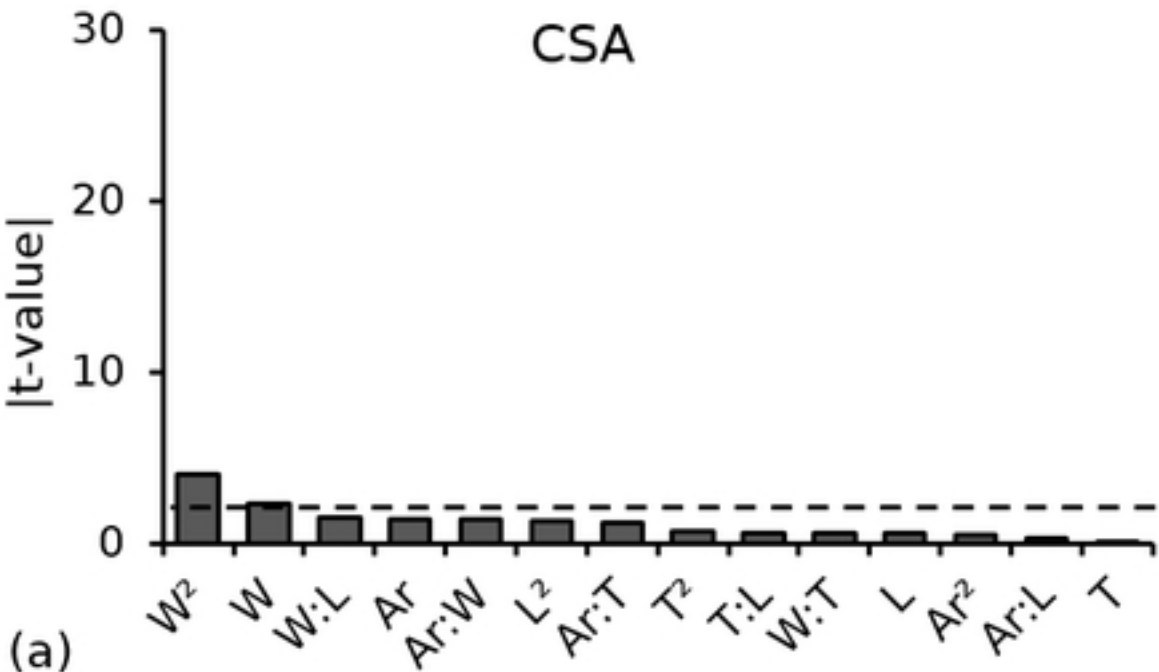
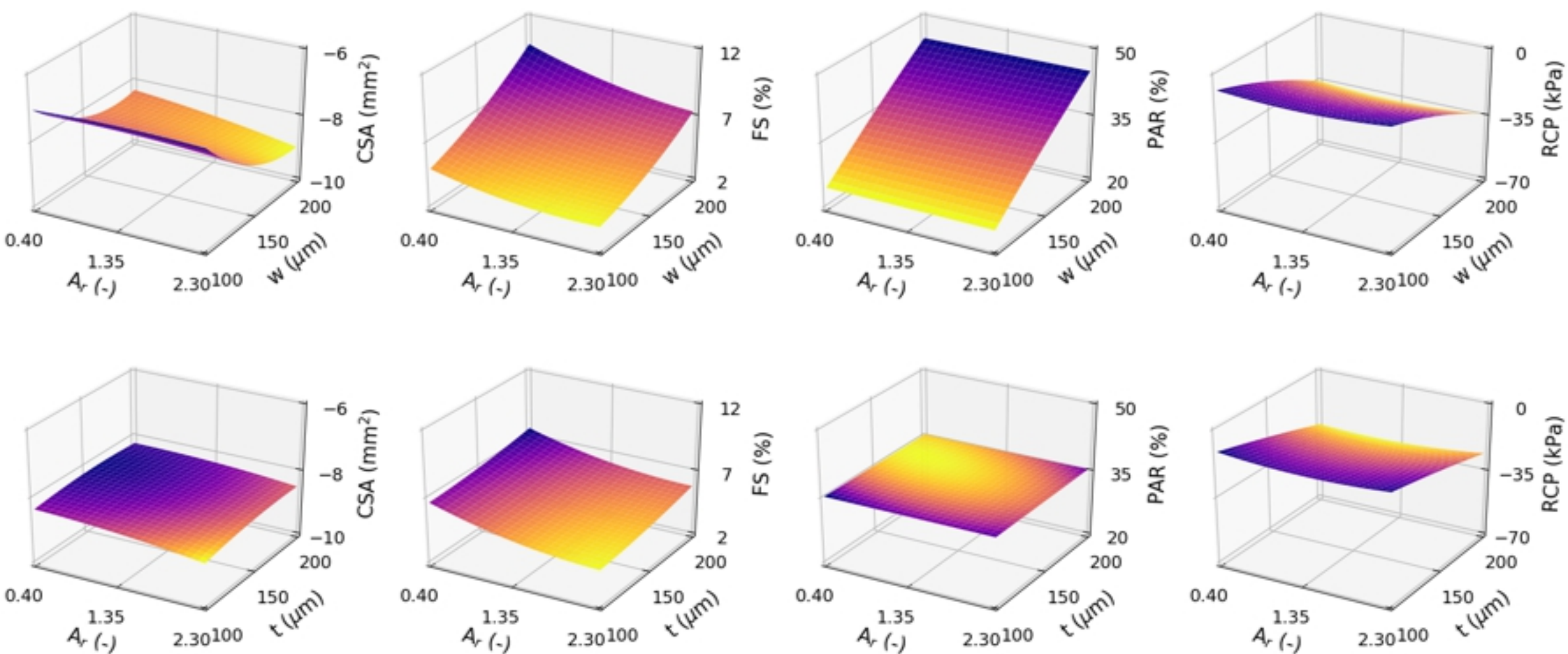


Figure 9



bioRxiv preprint doi: <https://doi.org/10.1101/667915>; this version posted June 11, 2019. The copyright holder for this preprint (which was not certified by peer review) is the author/funder, who has granted bioRxiv a license to display the preprint in perpetuity. It is made available under aCC-BY 4.0 International license.

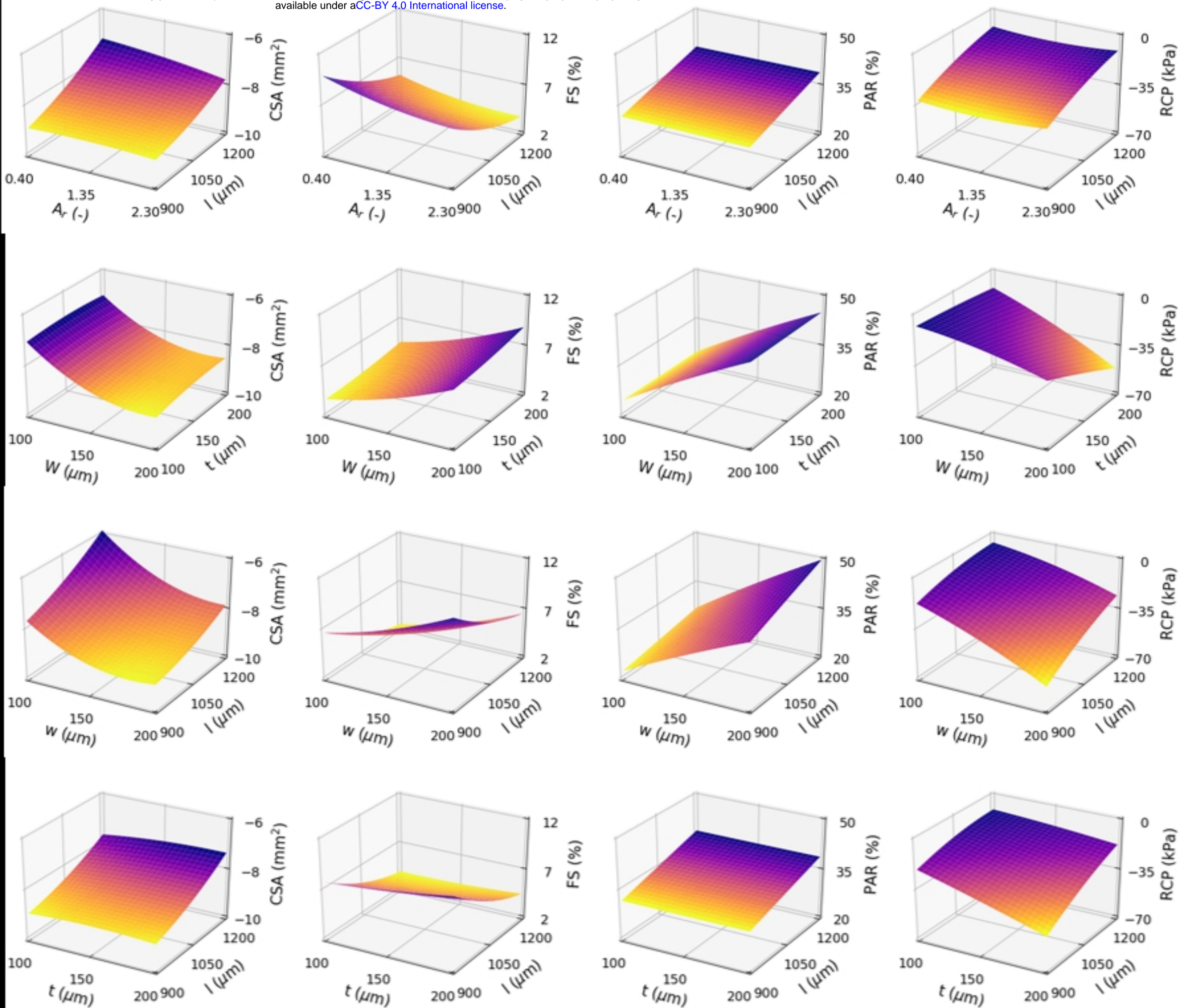


Figure 10

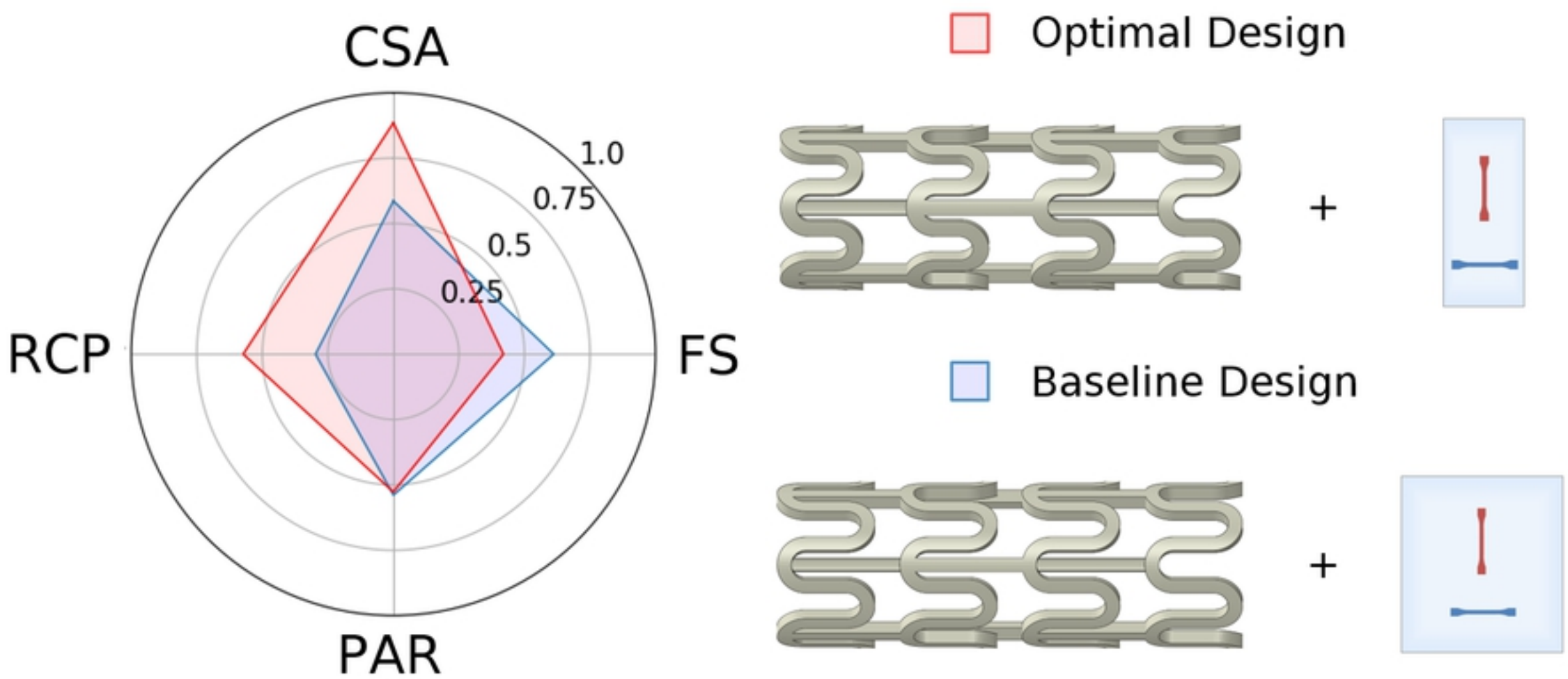


Figure 12